Global phase diagram of the cluster-XY spin chain with dissipation

Wei-Lin Li,[1,2] Ying-Ao Chen,[3] Zheng-Xin Guo,[4,*] Xue-Jia Yu,[5,6,†] and Zhi Li[1,2,‡]

[1]*Key Laboratory of Atomic and Subatomic Structure and Quantum Control (Ministry of Education), Guangdong Basic Research Center of Excellence for Structure and Fundamental Interactions of Matter, School of Physics, South China Normal University, Guangzhou 510006, China*

[2]*Guangdong Provincial Key Laboratory of Quantum Engineering and Quantum Materials, Guangdong-Hong Kong Joint Laboratory of Quantum Matter, Frontier Research Institute for Physics, South China Normal University, Guangzhou 510006, China*

[3]*DongGuan Experimental Middle School, Dongguan 523007, China*

[4]*Wilczek Quantum Center and Key Laboratory of Artificial Structures and Quantum Control, School of Physics and Astronomy, Shanghai Jiao Tong University, Shanghai 200240, China*

[5]*Department of Physics, Fuzhou University, Fuzhou, Fujian 350116, China*

[6]*Fujian Key Laboratory of Quantum Information and Quantum Optics, College of Physics and Information Engineering, Fuzhou University, Fuzhou, Fujian 350108, China*

(Received 11 October 2024; accepted 10 January 2025; published 24 January 2025)

We study the ground-state phase diagram of a non-Hermitian cluster-XY spin chain in the language of free fermions. By calculating the second derivative of ground-state energy density and various types of order parameters, we establish the global ground-state phase diagram of the model, exhibiting rich quantum phases and corresponding phase transitions. Specifically, the results reveal that the non-Hermitian cluster-XY model contains five different phases and two critical regions, i.e., ferromagnetic (FM), antiferromagnetic (AFM), symmetry-protected topological (SPT), paramagnetic (PM), Luttinger liquid-like phase, as well as critical regions I and II. The order parameters and critical behaviors are investigated and the correctness of the theory is confirmed.

DOI: 10.1103/PhysRevA.111.013316

I. INTRODUCTION

With the ever-evolving ultracold atomic technology, optical lattice-based quantum simulation of ultracold atomic system has made rapid progress [1–8]. Due to high controllability and purity, ultracold atomic systems are widely used to simulate phase transitions in condensed matter systems [3,9–16]. Recently, due to its unique symmetry-protected topological (SPT) phase, the cluster spin model based on ultracold atoms in triangular lattices has received extensive attention [17–21]. A striking feature of this system is the coexistence of three-spin and two-spin couplings, and the competition between which will give rise to an exotic continuous quantum phase transition (QPT). In concrete terms, a phase transition from the SPT cluster phase to the symmetry-breaking phase occurs in the system [22–32]. In the past few years, a series of models containing such continuous phase transitions have been studied, such as the cluster-Ising model, cluster-XY model, and so on. The relevant ground-state phase diagrams have also been obtained one by one [23–27,29,33,34]. Furthermore, some topological properties of the cluster spin model have been found, such as symmetry-protected edge modes at the gapped cluster SPT state and symmetry-enriched or topological nontrivial quantum critical points (QCPs) [28–32,35].

However, dissipation of the system is inevitable in almost all experimental platforms, be it a condensed matter platform or an artificial quantum simulation system [36–40], or trapped ions [41–43]. Therefore, dissipation is a factor that must be taken into account. It is also for this reason that many recent studies discussed dissipative non-Hermitian systems. In addition to the experimental requirements, considering that dissipative non-Hermitian systems also have some unique properties that cannot be found in traditional Hermitian systems, for instance, the non-Hermitian skin effect [38,44–46], non-Hermitian chiral properties [47–49], exception points [50–52], spawning rings [53], mobility edge [54,55], and so on. Recently, non-Hermitian physics has witnessed continuous progress and significant theoretical milestones [54,56–65] including the hot topic of non-Hermitian topology [66–73] and the nature of non-Hermitian exception points [50–52].

So far, although both SPT and non-Hermitian studies have come under the spotlight, few efforts explored the properties of non-Hermitian SPT systems by combining the two. This work is devoted to the ground-state properties and phase transitions of the dissipative cluster-XY model. We will construct a non-Hermitian cluster-XY model by introducing a complex field. Then, by the second derivative of the ground-state energy density, we show the non-Hermitian phase diagram.

The rest of this paper is organized as follows. In Sec. II, we introduce the model and study the corresponding ground

*Contact author: zx_guo@sjtu.edu.cn
†Contact author: xuejiayu815@gmail.com
‡Contact author: lizphys@m.scnu.edu.cn

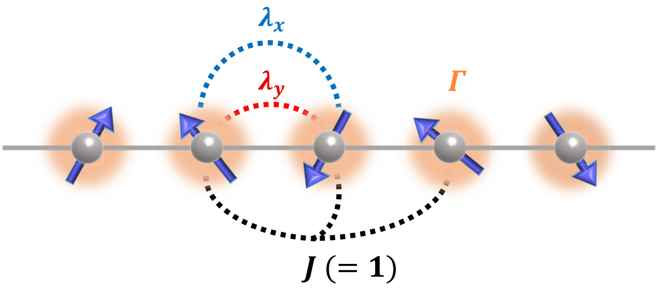

FIG. 1. Graphic demonstration of the cluster-XY model with dissipation, where λ_x and λ_y are the Ising exchange strength in the x and y directions, respectively. J is the strength of cluster term. Γ is the dissipation strength. Throughout, we set $J = 1$.

states by the analytical calculations. Then, we overview the phase diagram in Sec. IV. We calculate the energy gap and various types of order parameters in Sec. V to identify different phases. In Sec. VI, we investigate the phase transitions and critical behaviors. We summarize this paper in Sec. VII.

II. MODEL AND ANALYTICAL SOLUTION

We start with a dissipative cluster-XY model represented by an effective Hamiltonian with a complex field (see Appendix A for details). The corresponding Hamiltonian reads

$$H_{\text{eff}} = -J\sum_{l=1}^{N}\sigma_{l-1}^{x}\sigma_{l}^{z}\sigma_{l+1}^{x} + \lambda_x\sum_{l=1}^{N}\sigma_{l}^{x}\sigma_{l+1}^{x} + \lambda_y\sum_{l=1}^{N}\sigma_{l}^{y}\sigma_{l+1}^{y} - \frac{i\Gamma}{2}\sum_{l=1}^{N}\sigma_{l}^{u}, \quad (1)$$

where $\sigma_l^{\alpha}(\alpha = x, y, z)$ is the Pauli matrix of the lth spin. $\sigma^u = [\begin{smallmatrix}1 & 0\\ 0 & 0\end{smallmatrix}]$ denotes the loss or gain effect, which can be conveniently realized in optical systems and optical lattice ultracold atomic systems [72,74,75]. Without loss of generality, we take $J = 1$ as the unit of energy in the following calculation. Experimentally, there are three controllable parameters, namely, the spin exchange strengths λ_x, λ_y and the dissipation strength Γ (see Fig. 1).

One can transform Eq. (1) into fermionic representation by conducting a Jordan-Wigner transformation, which is defined as

$$\sigma_l^z = 1 - 2c_l^{\dagger}c_l, \quad (2)$$

$$\sigma_l^{+} = \prod_{j<l}(1 - 2c_j^{\dagger}c_j)c_l, \quad (3)$$

where $c_l^{\dagger}(c_l)$ is the creation (annihilation) operator at site l. Then, one can perform the Fourier transform

$$c_l = \frac{e^{-i\pi/4}}{\sqrt{N}}\sum_k e^{-ikl}c_k. \quad (4)$$

Then, we obtain

$$H = \sum_k [y_k(c_k^{\dagger}c_{-k}^{\dagger} + c_{-k}c_k) + z_k(c_k^{\dagger}c_k + c_{-k}^{\dagger}c_{-k} - 1)], \quad (5)$$

where $y_k = -\sin(2k) - (\lambda_y - \lambda_x)\sin(k)$ and $z_k = -\cos(2k) + (\lambda_x + \lambda_y)\cos(k) - \frac{i\Gamma}{4}$. By using the Bogoliubov transformation

$$\gamma_k = u_k c_k + v_k c_{-k}^{\dagger}, \quad \bar{\gamma}_k = u_k c_k^{\dagger} + v_k c_{-k}. \quad (6)$$

Eventually, we get the diagonalized Hamiltonian

$$H = \sum_k \Lambda_k\left(\bar{\gamma}_k\gamma_k - \frac{1}{2}\right), \quad (7)$$

where

$$\Lambda_k = 2\sqrt{y_k^2 + z_k^2}. \quad (8)$$

In this work, we define the ground state as the state with the minimum real part of Λ_k. The ground state of Eq. (1) is

$$|G\rangle = \frac{1}{\sqrt{N}}\prod_{k>0}[u_k - v_k c_k^{\dagger}c_{-k}^{\dagger}]\,|0\rangle\,, \quad (9)$$

where $N = \prod_{k>0}(|u_k|^2 + |v_k|^2)$ is the normalization constant, $u_k = \frac{-z_k - \sqrt{y_k^2 + z_k^2}}{C}$, $v_k = \frac{y_k}{C}$, and C is a constant to satisfy $u_k^2 + v_k^2 = 1$.

III. OBSERVABLES AND METHODS

A. Ground-state energy density and its second-order derivative

According to Eq. (8), the ground-state energy density can be defined as

$$e_0 = -\frac{1}{N}\sum_k \Lambda_k = -\frac{1}{\pi}\int_0^{\pi}\sqrt{y_k^2 + z_k^2}\,dk, \quad (10)$$

and we can easily obtain the second derivative of e_0 with respect to λ_x, i.e., $-\frac{\partial^2 e_0}{\partial \lambda_x^2}$.

B. Energy gap

In Hermitian cases, the minimum value of Λ_k is defined as the energy gap, which is usually labeled as Δ, i.e.,

$$\Delta = \min_k \Lambda_k. \quad (11)$$

The place where the energy gap closes ($\Delta = 0$) is usually the critical point of the phase transition. In non-Hermitian cases, however, since the value of Λ_k is complex, the gap of the corresponding emergent phases is complex. Therefore, for the non-Hermitian case, we must examine both the real and imaginary parts of the energy gap, which are labeled as Re[Δ], Im[Δ], respectively.

C. Order parameters

To identify each phase, we calculate the spin correlation function and string order parameter, which are two key quantities to study the cluster spin model [22]. The spin correlation function is defined as

$$R_{\alpha}(r) = \langle\sigma_j^{\alpha}\sigma_l^{\alpha}\rangle, \quad (12)$$

where $r = j - l, \alpha = x,\ y,\ z$. Then, one can obtain

$$R_x(r) = \left\langle (c_j - c_j^\dagger) \prod_{j<m<l} (1 - 2c_m^\dagger c_m)(c_l^\dagger + c_l) \right\rangle = \langle B_j A_{j+1} B_{j+1} \dots A_{l-1} B_{l-1} A_l \rangle, \quad (13)$$

$$R_y(r) = (-1)^r \langle A_j B_{j+1} A_{j+1} \dots B_{l-1} A_{l-1} B_l \rangle, \quad (14)$$

where $A_j = c_j^\dagger + c_j, B_j = c_j - c_j^\dagger$. There are pair contractions for A_j and B_j, i.e.,

$$Q_r = \langle A_j A_l \rangle = \delta_{jl} + \frac{1}{\pi} \int_0^\pi dk \left(\frac{u_k v_k^* - u_k^* v_k}{|u_k|^2 + |v_k|^2} \right) \sin(kr), \quad (15)$$

$$S_r = \langle B_j B_l \rangle = -\delta_{jl} + \frac{1}{\pi} \int_0^\pi dk \left(\frac{u_k v_k^* - u_k^* v_k}{|u_k|^2 + |v_k|^2} \right) \sin(kr), \quad (16)$$

$$\begin{aligned} G_r = -D_{-r} &= \langle B_j A_l \rangle \\ &= -\frac{1}{\pi} \int_0^\pi dk \left(\frac{|u_k|^2 - |v_k|^2}{|u_k|^2 + |v_k|^2} \right) \cos(kr) \\ &\quad + \frac{1}{\pi} \int_0^\pi dk \left(\frac{u_k v_k^* - u_k^* v_k}{|u_k|^2 + |v_k|^2} \right) \sin(kr), \end{aligned} \quad (17)$$

where $r = l - j$ [76]. Since both $R_x(r)$ and $R_y(r)$ contain a lot of operators, it is useful to write them in terms of the Pfaffian of a skew-symmetric matrix [77,78], i.e.,

$$R_x(r) = \mathrm{Pf} \begin{vmatrix} 0 & G_1 & S_1 & G_2 & S_2 & \cdots & G_r \\ & 0 & D_0 & Q_1 & D_1 & \cdots & Q_{r-1} \\ & & 0 & G_1 & S_1 & \cdots & G_{r-1} \\ & & & 0 & D_0 & \cdots & Q_{r-2} \\ & & & & \ddots & \ddots & \vdots \\ & & & & & 0 & G_1 \\ & & & & & & 0 \end{vmatrix}, \quad (18)$$

$$R_y(r) = (-1)^{r+1} \mathrm{Pf} \begin{vmatrix} 0 & D_1 & Q_1 & D_2 & Q_2 & \cdots & D_r \\ & 0 & G_0 & S_1 & G_1 & \cdots & S_{r-1} \\ & & 0 & D_1 & Q_1 & \cdots & D_{r-1} \\ & & & 0 & G_0 & \cdots & S_{r-2} \\ & & & & \ddots & \ddots & \vdots \\ & & & & & 0 & D_1 \\ & & & & & & 0 \end{vmatrix}. \quad (19)$$

The string order parameter can be calculated in the same way as the spin correlation function. Then, we have

$$O^x = \lim_{r \to \infty} (-1)^r \left\langle \sigma_1^x \sigma_2^y \left(\prod_{k=3}^{r} \sigma_k^z \right) \sigma_{r+1}^y \sigma_{r+2}^x \right\rangle. \quad (20)$$

Similarly, by using $A_j = c_j^\dagger + c_j$ and $B_j = c_j - c_j^\dagger$, we can obtain

$$O^x = \lim_{r \to \infty} \langle B_1 B_2 A_3 B_3 A_4 B_4 \dots A_r B_r A_{r+1} A_{r+2} \rangle. \quad (21)$$

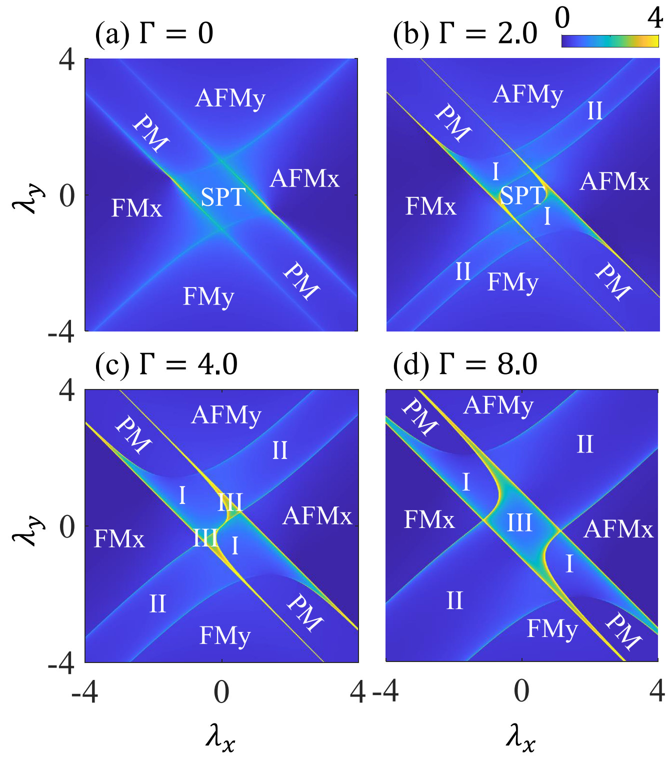

FIG. 2. The phase diagrams characterized by the real part of the second derivative of ground-state energy density $-\frac{\partial^2 e_0}{\partial \lambda_x^2}$ for (a) $\Gamma = 0$, (b) $\Gamma = 2.0$, (c) $\Gamma = 4.0$, and (d) $\Gamma = 8.0$.

Similarly, O^x can be converted to a Pfaffian of a skew-symmetric matrix, i.e.,

$$O^x(r) = \mathrm{Pf} \begin{vmatrix} 0 & S_1 & G_2 & S_2 & G_3 & S_3 & \cdots & G_{r+1} \\ & 0 & G_1 & S_1 & G_2 & S_2 & \cdots & G_r \\ & & 0 & D_0 & Q_1 & D_1 & \cdots & Q_{r-1} \\ & & & 0 & G_1 & S_1 & \cdots & G_{r-1} \\ & & & & 0 & D_0 & \cdots & Q_{r-2} \\ & & & & & \ddots & \ddots & \vdots \\ & & & & & & 0 & Q_1 \\ & & & & & & & 0 \end{vmatrix}. \quad (22)$$

It is worth noting that r should be as large as possible in the numerical calculation to approach the thermodynamic limit.

The string order parameter O^x tends to be a constant in the nontrivial cluster SPT phase, and decays exponentially in FM, AFM, and PM phases [79–82]. The spin correlation functions $|R_x(r)|$ and $|R_y(r)|$ tend to be a fixed nonzero constant in the AFM phase along x or y direction, while they decay exponentially to zero in the disordered PM phase.

IV. PHASE DIAGRAM

The schematic phase diagram is provided in Fig. 2.

Let's briefly outline the corresponding phase diagram and summarize the main findings.

Under the condition of $\Gamma = 0$, the model is reduced to the nondissipative case, i.e., the standard cluster-XY model,

TABLE I. The energy gap and long-distance behaviors of order parameters in different phases and critical regions.

	Δ	$\|O^x\|$	$\|R_x\|$	$\|R_y\|$
SPT	real	constant	0	0
PM	real	exponential decay	exponential decay	exponential decay
$FM_x(AFM_x)$	real	exponential decay	constant	exponential decay
$FM_y(AFM_y)$	real	exponential decay	exponential decay	constant
Critical region I	0	power-law decay	oscillating decay as r^{-a}	exponential decay
Critical region II	imaginary	exponential decay	power-law decay	power-law decay
Luttinger liquid-like phase	imaginary	power-law decay	oscillating decay as r^{-a}	oscillating decay as r^{-a}

whose phase diagram is shown in Fig. 2(a). However, the introduction of dissipation will bring about great changes in the phase diagram of the system. Specifically, when dissipation strength Γ is weak, the SPT region will gradually shrink and two types of critical regions will appear in the system, namely, region I and region II [see Fig. 2(b)]. With a further increase in dissipation strength Γ, the SPT region will completely disappear [see Fig. 2(c)], and a new type of phase III, the Luttinger liquid-like phase, will emerge from the system. Specifically, the SPT phase vanishes completely under the condition of $\Gamma = 4$ (see Appendix B for details). After that, the region corresponding to phase III will increase with the ever-growing Γ [see Figs. 2(c) and 2(d)].

The details of these emergent phases are briefly outlined below.

(1) In critical region I, both the real part and imaginary part of the energy gap are zero. As the distance r increases, the string order parameter $|O^x(r)|$ shows a power-law decay, the spin correlation function $|R_y|$ decays exponentially, and $|R_x|$ presents an oscillating decay as r^{-a} (a is a constant).

(2) In critical region II, the energy gap is a purely imaginary number. With the distance r increasing, the string order parameter $|O^x(r)|$ decays exponentially, the spin correlation function $|R_x|$, $|R_y|$ features power-law decay.

(3) In the Luttinger liquid-like phase, the energy gap is a pure imaginary number. As the distance r increases, the string order parameter $|O^x(r)|$ shows a power-law decay and the spin correlation function $|R_y|$, $|R_x|$ presents an oscillating decline as r^{-a}.

The corresponding properties of different phases are summarized in the following Table I. The phase transitions both from the critical region I to AFM_x and from the Luttinger liquid-like phase to critical region II are first-order phase transitions. Furthermore, min $|\Lambda_k|$ is an effective tool for detecting the continuous phase transition in the non-Hermitian cluster-XY model. In the following sections, we will prove each of the above conclusions.

V. EMERGENT GAPLESS PHASES WITH DISSIPATION

Now, we explore the possible phases that appear in the phase diagram. Under the condition of $\Gamma = 0$, the model is a standard cluster-XY model. By adjusting the parameters λ_x, λ_y, the model contains four different phases, i.e., ferromagnetic (FM), antiferromagnetic (AFM), symmetry-protected topological (SPT), and paramagnetic (PM) [83]. However, when $\Gamma \neq 0$, new phases emerge [see Fig. 2].

To investigate the energy gap in each phases, we plot the real (top row) and imaginary (bottom row) parts of the energy gap in Fig. 3. Under the condition of $\Gamma = 0$, the Re[Δ] of different phase are all nonzero. The regions I, II, and III emerge and expand with an increasing Γ, and Re[Δ] of these three emergent phases are zero [see Figs. 3(b1) to 3(d1)]. The imaginary part, Im[Δ], is zero in region I, whereas it is nonzero in regions II and III. This is to say, the region I is a gapless phase, whereas both regions II and III are the imaginary-gapped phases [see Figs. 3(b2) to 3(d2)].

Now, we exhibit a detailed analysis of the long-distance behaviors of order parameters.

First, we set $\lambda_x = 0$. Under the condition of $\Gamma = 0$, one can find that, when $\lambda_y > 1$, the string order parameter $|O^x|$ tends to be zero and the spin correlation function $|R_y|$ tends to be a constant, which means the corresponding region is the AFM_y phase [see Figs. 4(a1) and 4(a2)]. When $\lambda_y = 0$, the string order parameter $|O^x|$ tends to a constant and $|R_y|$ tends to be zero, which means the corresponding region is the cluster SPT phase under such a circumstance.

Under the condition of $\Gamma = 2.0$, the order parameters' long-range behaviors become very different. For the case of $\lambda_y = 2$, the string order parameter $|O^x(r)|$ shows an exponential decay to be zero, whereas the spin correlation function $|R_y(r)|$ remains constant, indicating that the system resides in the AFM_y phase [see Figs. 4(b1) and 4(b2)]. In the middle region ($\lambda_y = 0$), the string order parameter $|O^x(r)|$ or the spin correlation function $|R_y(r)|$ becomes constant or tends to zero in the long-distance limit, confirming that this region is in the cluster SPT phase [see Figs. 4(b1) and 4(b2)]. However, $|O^x(r)|$ shows a power-law decay when $\lambda_y = 0.8$ [see Fig. 4(b1)], suggesting the presence of a quasi-long-range string order in region I. Then, as depicted in Fig. 4(b2), one can observe that $|R_y(r)|$ features the power-law decay, implying the existence of quasi-long-range AFM_y order in region II.

Under the condition of $\Gamma = 8.0$, as shown in the Fig. 4(c1), in region III ($\lambda_y = 0$), the string order parameter $|O^x(r)|$ shows a power-law decay as r increases, suggesting the existence of a quasi-long-range string order. In addition, one can observe that the spin correlation function $|R_y|$ presents an oscillating decline as r^{-a} in region III [see Fig. 4(c2)].

Second, we set $\lambda_y = 0$. When $\Gamma = 0$, as can be seen in Figs. 5(a1) and 5(a2), when $\lambda_x > 1$, the string order parameter $|O^x|$ or the spin correlation function $|R_x|$ tends to be zero or remains a constant value, confirming that the region is in the AFM_x phase. As depicted in Fig. 5(b1), the string order parameter $|O^x(r)|$ also shows a power-law decay in region

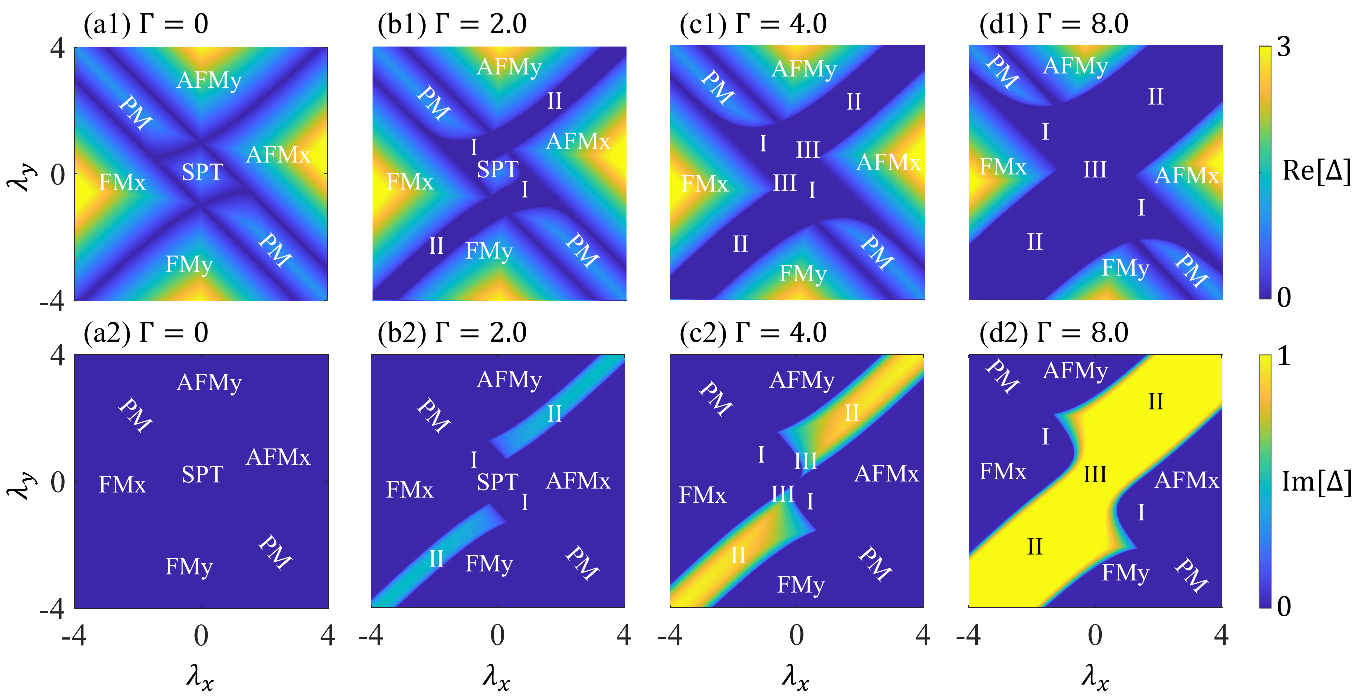

FIG. 3. The phase diagrams characterized by the real (top row) and imaginary (bottom row) parts of the energy gap for $\Gamma = 0$, 2.0, 4.0, 8.0.

I ($\lambda_x = 0.8$). Interestingly, in region I, $|R_x(r)|$ presents an oscillating decline as the distance r increases [see Fig. 5(b2)], which is consistent with its behavior at the SPT-PM phase transition point when $\Gamma = 0$ [see Fig. 7(a)]. So region I is a critical region which emerges from the SPT-PM phase transition line with an increasing dissipative strength Γ.

When $\Gamma = 8$, according to Fig. 5(c2), one can observe that $|R_x(r)|$ shows the power-law decay in the critical region II, which is consistent with its behavior at the AFM_x-AFM_y phase transition point when $\Gamma = 0$ [see Fig. 7(b)]. So one can consider that region II is a critical region emerging from AFM_x-AFM_y phase transition line with an increasing dissipative strength Γ. More discussion about the critical regions is in Appendix C. As depicted in the inset of Fig. 5(c2), the spin correlation function $|R_x|$ presents an oscillating decline as r^{-a} in region III. Combining the long-distance behaviors of $|O^x|$ and $|R_y|$ shown in Figs. 4(c1) and 4(c2), we define that the region III is a Luttinger liquid-like phase. In addition, we also investigate the long-distance behaviors of correlation functions in PM phase (see Appendix D for details).

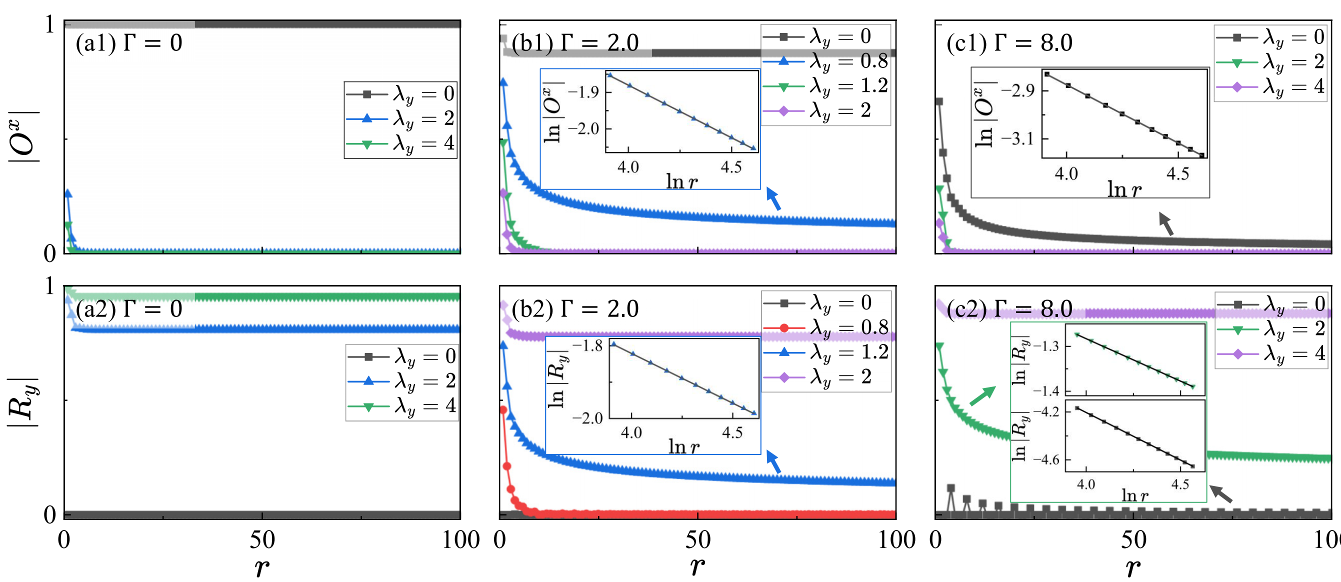

FIG. 4. The long-distance behaviors of string order parameter $|O^x|$ and spin correlation function $|R_y|$ for (a1), (a2) $\Gamma = 0$, (b1), (b2) $\Gamma = 2.0$, as well as (c1), (c2) $\Gamma = 8.0$. These insets show that the order parameters exhibit the power-law decay as r increases. Specifically, the inset which contains black square in (c2) shows that spin correlation function $|R_y|$ presents an oscillating decline as $r^{-0.7943}$. Throughout, $\lambda_x = 0$.

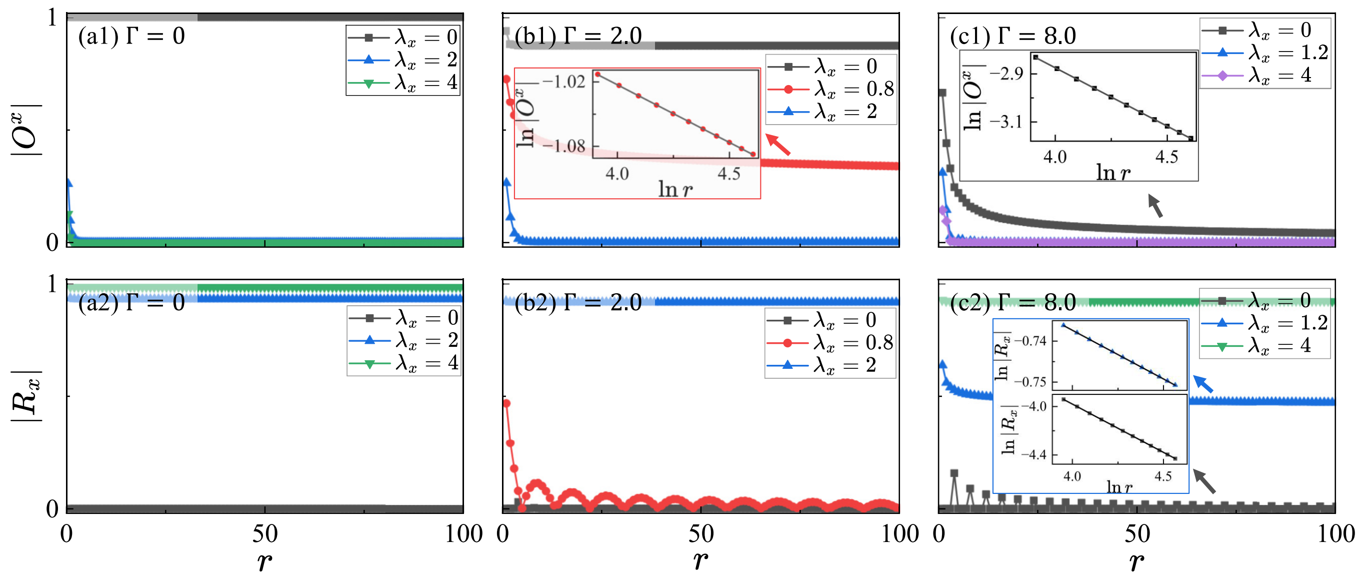

FIG. 5. The long-distance behaviors of string order parameter $|O^x|$ and spin correlation function $|R_x|$ for (a1), (a2) $\Gamma = 0$, (b1), (b2) $\Gamma = 2.0$, as well as (c1), (c2) $\Gamma = 8.0$. These insets show that the order parameters exhibit the power-law decay as r increases. Specifically, the inset which contains the black square in (c2) shows that spin correlation function $|R_x|$ presents an oscillating decline satisfying $r^{-0.7973}$. Throughout, $\lambda_y = 0$.

We summarize the corresponding properties of the energy gap and correlation functions of different phases and critical regions in Table I.

However, we set $\lambda_x = 0$, $r = 1000$, and study the distribution of the order parameters under different dissipative strengths. In the Hermitian case [see Fig. 6(a)], when $\lambda_y > 1$ ($\lambda_y < 1$), $|R_y|$ is nonzero, indicating that the system resides in the $\mathrm{AFM_y}$($\mathrm{FM_y}$) phase in such a parameter region. When $-1 < \lambda_y < 1$, $|O^x|$ is nonzero, suggesting that the region is in the cluster SPT phase. Then we investigate the non-Hermitian case. As depicted in Fig. 6(b), when $\Gamma = 2.0$, one can observe that $|R_y|$ is a constant in critical region II and $|O^x|$ is a constant in critical region I. As dissipative strength Γ increases from 2.0 to 4.0, the SPT phase narrows, while critical region I,

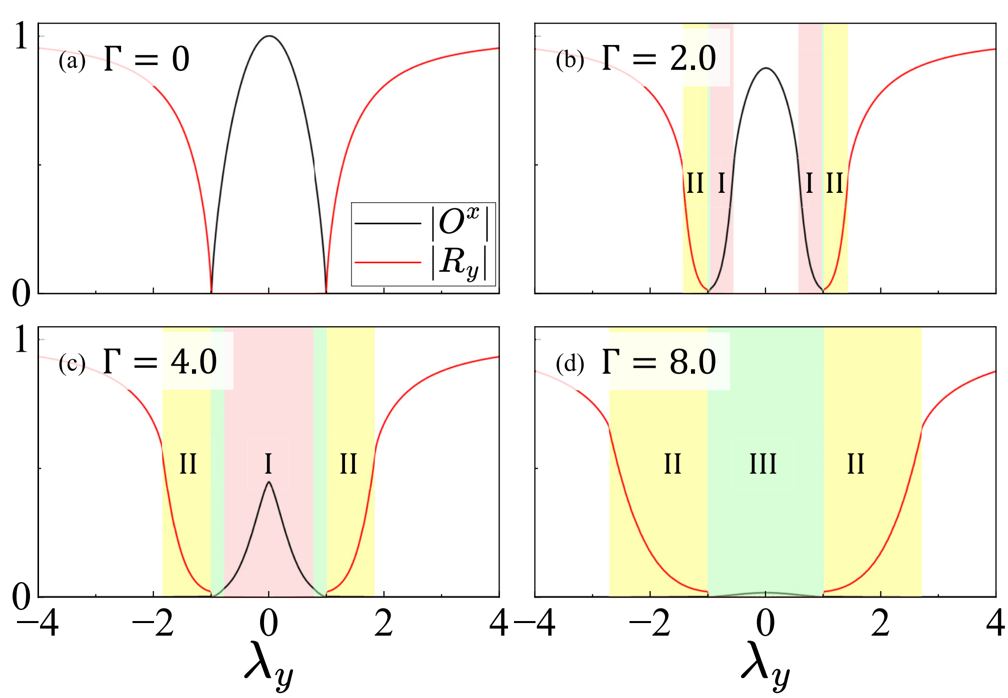

FIG. 6. The numerical results of string order parameter $|O^x|$, spin correlation function $|R_y|$ with respect to λ_y for (a) $\Gamma = 0$, (b) $\Gamma = 2.0$, (c) $\Gamma = 4.0$, and (d) $\Gamma = 8.0$. The red, yellow, and green shadings correspond to critical regions I, II, and Luttinger liquid-like phase, respectively. Throughout, $\lambda_x = 0$, $r = 1000$.

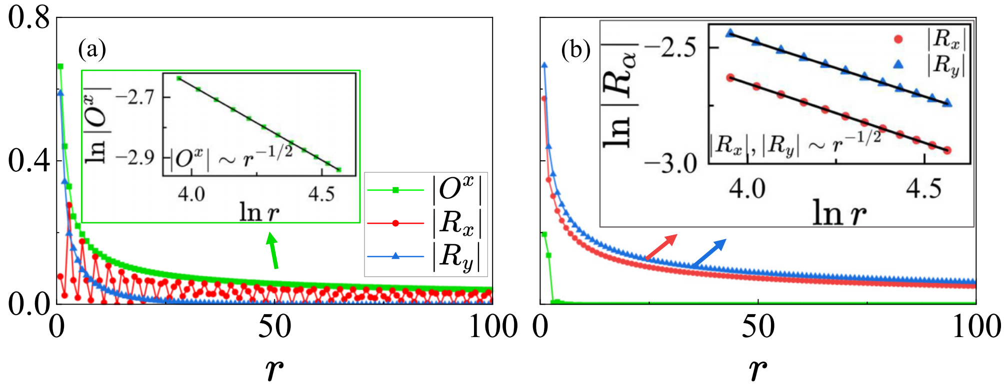

FIG. 7. The long-distance behaviors of string order parameter $|O^x|$ and spin correlation function $|R_x|$, $|R_y|$ for (a) $\lambda_x = 0.1,\ \lambda_y = -0.9512$ and (b) $\lambda_x = 3.0,\ \lambda_y = 3.3030$. Throughout, $\Gamma = 0$.

critical region II, and the Luttinger liquid-like phase expand [see Figs. 6(b) and 6(c)]. When Γ increases to 4.0, the region of the SPT phase disappears completely [see Fig. 6(c)]. As the dissipative strength Γ further increases, the critical region II and Luttinger liquid-like phase continuously expand [see Fig. 6(d)]. Additionally, we investigate the distribution of the order parameters under different dissipative strengths when $\lambda_y = 0$ (see Appendix E for details).

VI. PHASE TRANSITIONS AND CRITICAL BEHAVIORS

After delineating all the quantum phases in the phase diagram, we shift our focus to the more intriguing QPTs between these phases. In this section, we are ready to investigate phase transitions and critical behaviors.

By means of the second derivative of e_0 calculations, one can observe that the second derivative of the ground-state energy density $-\frac{\partial^2 e_0}{\partial \lambda_x^2}$ becomes sharper at critical points [see Fig. 2]. When $\Gamma \neq 0$, some new phase transition lines emerge [see Fig. 2]. One can observe that critical region I and critical region II emerge from the transition line of the SPT-PM and $\mathrm{AFM_y}$-$\mathrm{AFM_x}$ phase in the Hermitian case. So to explain the properties of critical region I and critical region II, we investigate the properties of correlation functions at the critical points of SPT-PM and $\mathrm{AFM_y}$-$\mathrm{AFM_x}$ transitions when $\Gamma = 0$.

The numerical results are depicted in Fig. 7. As shown in Fig. 7(a), the string order parameter $|O^x|$ shows a power-law decay, the spin correlation function $|R_x|$ shows oscillating decay as r^{-a}, and $|R_y|$ decays exponentially at the critical point of the SPT-PM transitions. These long-distance behaviors of the correlation functions are the same as those in critical region I. The inset shows that the slope of curves in the ln-ln plot is $-1/2$, implying that the critical exponent η of SPT-PM transitions is $1/2$ [see Fig. 7(a)]. Then, one can observe that the spin correlation function $|R_x|$, $|R_y|$ shows power-law decay and the string order parameter $|O^x|$ exhibits an exponential decay at the critical point of the $\mathrm{AFM_y}$-$\mathrm{AFM_x}$ transitions [see Fig. 7(b)]. These long-distance behaviors of the correlation functions are consistent with the properties of the correlation functions in the critical region II. The inset shows that the slope of the curves in the ln-ln plot is $-1/2$, implying that the critical exponent η of the $\mathrm{AFM_y}$-$\mathrm{AFM_x}$ transitions is $1/2$.

However, to determine whether the phase transition is a first-order phase transition, we study the scaling behaviors of the order parameters at the QCPs. The numerical results are presented in Fig. 8. One can observe that the jump in the spin correlation function $|R_x|$ at critical region I-$\mathrm{AFM_x}$ transitions and another jump at the Luttinger liquid-like phase-critical region II transitions, which indicate that the transitions of both critical region I-$\mathrm{AFM_x}$ and the Luttinger liquid-like phase-critical region II are first-order phase transitions [see Fig. 8]. Combining with the previous numerical results of the energy gap [see Fig. 3], we can discover that the points where $\mathrm{Re}[\Delta] = 0$ and the points where $\mathrm{Im}[\Delta] = 0$ do not correspond to phase transition points completely. Interestingly, one

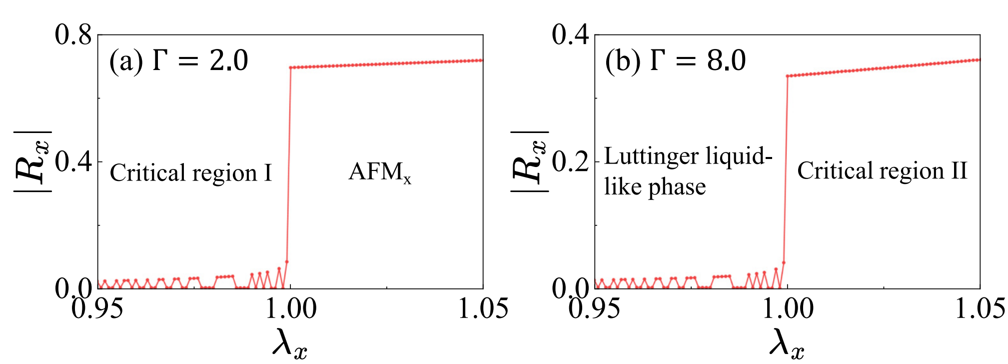

FIG. 8. The spin correlation function $|R_x|$ with respect to λ_x for (a) $\Gamma = 2.0$ and (b) $\Gamma = 8.0$. Throughout, $\lambda_y = 0$, $r = 1000$.

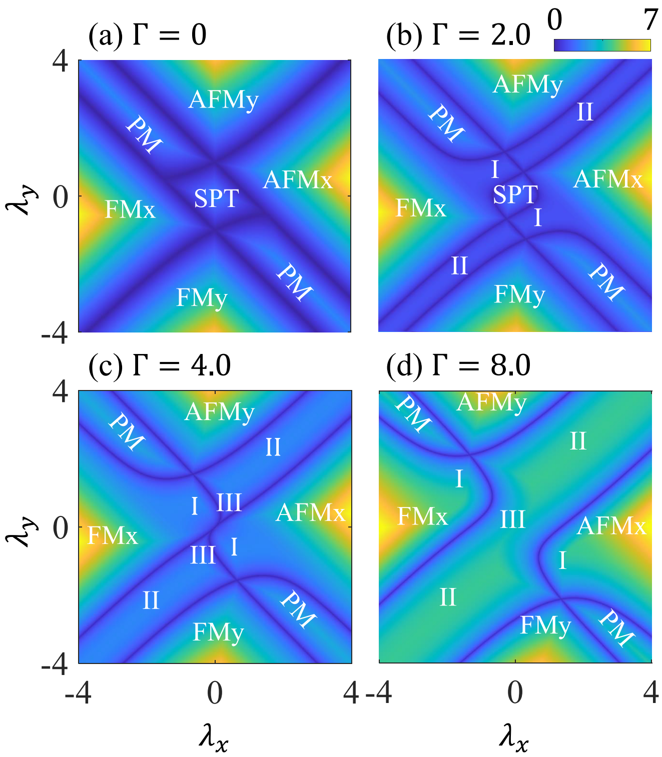

FIG. 9. The phase diagrams characterized by $\min|\Lambda_k|$ for (a) $\Gamma = 0$, (b) $\Gamma = 2.0$, (c) $\Gamma = 4.0$, and (d) $\Gamma = 8.0$.

can discover that the points of $\min|\Lambda_k| = 0$ correspond to the continuous phase transitions in our system [see Fig. 9].

VII. SUMMARY

In summary, we investigate the effect of dissipation on the phase diagram of the cluster-XY model. By means of the second derivative of the ground-state energy density calculation, we can observe that the introduction of established field can destroy the SPT phase and emerge with three novel phases. By calculating the energy gap and order parameters, we obtain the properties of different phases and the critical behaviors at the points of the phase transitions. In critical region I, the string order parameter $|O^x|$ exhibits power-law decay, the spin correlation function $|R_y|$ decays exponentially, and $|R_x|$ presents an oscillating decay as r^{-a}, which are consistent with the critical behaviors of SPT-PM transitions. Different from critical region I, the string order parameter $|O^x(r)|$ decays exponentially, the spin correlation function $|R_x|$, $|R_y|$ features power-law decay in critical region II, which are consistent with the critical behaviors of the $\mathrm{AFM_x}-\mathrm{AFM_y}$ transitions. In the Luttinger liquid-like phase, the string order parameter $|O^x(r)|$ satisfies power-law decay and the spin correlation function $|R_y|$, $|R_x|$ presents oscillating decay as r^{-a}. Along with the emergent phases, the transitions of the critical region I-$\mathrm{AFM_x}$ and Luttinger liquid-like phase-critical region II are first-order phase transitions. Interestingly, continuous phase transitions occur with $\min|\Lambda_k| = 0$. Our series of theoretical work (Ref. [27] and this paper) will be a constant push to the ever-deepening research on novel phases and phase transitions in cluster spin system.

ACKNOWLEDGMENTS

We sincerely thank D.-W. Zhang for helpful discussions. This work was supported by the National Key Research and Development Program of China (Grant No. 2022YFA1405300). Z.L. was supported by Open Fund of Key Laboratory of Atomic and Subatomic Structure and Quantum Control (Ministry of Education). X.-J.Y. was supported by the National Natural Science Foundation of China (Grant No. 12405034).

APPENDIX A: EFFECTIVE NON-HERMITIAN HAMILTONIAN

In this section, we provide the calculation details about the non-Hermitian Hamiltonian in Eq. (1). The non-Hermitian Hamiltonian in Eq. (1) can be realized in the quantum trajectory approach [84–88]. Let us consider a Markovian open quantum system, which is generally described by the Lindblad master equation [89,90]

$$\frac{d}{dt}\hat{\rho} = -i[\hat{H}, \hat{\rho}] + \sum_l \left(\hat{L}_l\hat{\rho}\hat{L}_l^\dagger - \frac{1}{2}\{\hat{L}_l^\dagger\hat{L}_l, \hat{\rho}\}\right), \tag{A1}$$

where $\hat{\rho}$ is the density operator, $\hat{H}$ is the Hamiltonian that describes the coherent dynamics, and $\hat{L}_l$'s are the jump operators that describe the coupling to the external environment. This master equation can be written as

$$\frac{d}{dt}\hat{\rho} = -i(\hat{H}_{\mathrm{eff}}\hat{\rho} - \hat{\rho}\hat{H}_{\mathrm{eff}}^\dagger) + \sum_l \hat{L}_l\hat{\rho}\hat{L}_l^\dagger, \tag{A2}$$

with the effective non-Hermitian Hamiltonian

$$\hat{H}_{\mathrm{eff}} = \hat{H} - \frac{i}{2}\sum_l \hat{L}_l^\dagger\hat{L}_l. \tag{A3}$$

The term $\hat{L}_l\hat{\rho}\hat{L}_l^\dagger$ indicates each quantum trajectory subject to stochastic loss events. The term $-\frac{i}{2}\sum_l \hat{L}_l^\dagger\hat{L}_l$ is the dissipation term $\hat{H}_{\mathrm{dissipation}}$. Under continuous monitoring and postselection of the null measurement outcome (no-click limit), the dissipative dynamics is described by the effective non-Hermitian Hamiltonian $\hat{H}_{\mathrm{eff}}$. Here we choose the Hamiltonian $\hat{H}$ and the jump operators $\hat{L}_l$ to be

$$\hat{H} = -J\sum_{l=1}^{N}\sigma_{l-1}^x\sigma_l^z\sigma_{l+1}^x + \lambda_x\sum_{l=1}^{N}\sigma_l^x\sigma_{l+1}^x + \lambda_y\sum_{l=1}^{N}\sigma_l^y\sigma_{l+1}^y, \tag{A4}$$

$$\hat{L}_l = \sqrt{\Gamma}\sigma_l^-. \tag{A5}$$

So the effective Hamiltonian can be written as

$$\hat{H}_{\mathrm{eff}} = \hat{H} - \frac{i\Gamma}{2}\sum_l \sigma_l^u, \tag{A6}$$

where $\sigma^u = \left[\begin{smallmatrix}1 & 0\\ 0 & 0\end{smallmatrix}\right]$.

APPENDIX B: DETAILS ABOUT THE PHASE DIAGRAM UNDER DIFFERENT DISSIPATION STRENGTH Γ

In this section, we provide the phase diagrams under different dissipation strength Γ.

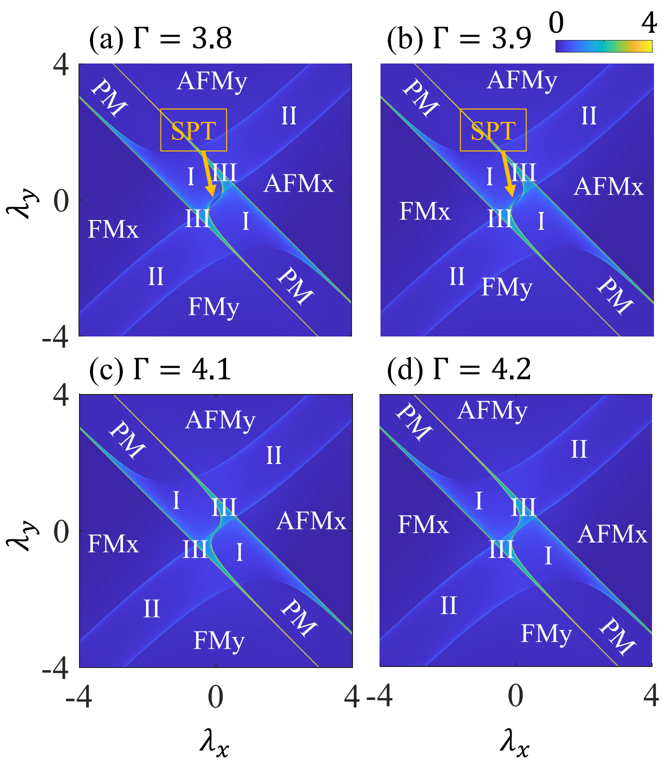

FIG. 10. The phase diagrams characterized by the real part of the second derivative of ground-state energy density $-\frac{\partial^2 e_0}{\partial \lambda_x^2}$ for (a) $\Gamma = 3.8$, (b) $\Gamma = 3.9$, (c) $\Gamma = 4.1$, and (d) $\Gamma = 4.2$.

As shown in Figs. 10(a) and 10(b), the results reveal that the area of the SPT phase located in the center of the phase diagram is very small. Comparing with the cases of $\Gamma = 2.0$ [see Fig. 2(b)], we can observe that the SPT region will gradually shrink with a further increase in dissipation strength Γ. Under the condition of $\Gamma = 4.1,\ 4.2$, we can observe that the SPT phase disappears [see Figs. 10(c) and 10(d)]. So the results reveal that the SPT phase vanishes completely under the condition of $\Gamma = 4$.

APPENDIX C: MORE DISCUSSION ABOUT THE CRITICAL REGIONS

According to Figs. 2(a) and 2(b), we can find that with an increasing Γ, critical regions I and II emerge from the SPT-PM and AFM_y-AFM_x phase transition lines. Our results reveal that the long distance behavior of the correlation function in critical regions I and II is consistent with its behavior at the SPT-PM, AFM_y-AFM_x phase transition lines, respectively. That is because the dissipation induces a critical phase, which behaves in the same way as the original phase transition point. Analogous to the quantum critical region at finite temperature [91], coupling of the system to the bath also leads to the emergence of the critical region. In our case, the coupling of the system to dissipation similarly induces the critical region, where the behaviors of the order parameter on the original phase transition lines control the behaviors of the order parameter in the critical region.

Furthermore, one can understand this phenomenon by comparing it with a finite-temperature quantum critical problem, where the zero-temperature quantum critical point extends to a critical region that shares the same critical behaviors. In both cases, the system is coupled to a huge bath, which leads to a quantum-critical-point-controlled quantum critical region. The authors of Ref. [60] also revealed that the critical behavior of the non-Hermitian system was similar to the critical point of phase transition in Hermitian system. All in all, this is a very interesting problem that we plan to further explore in our future work.

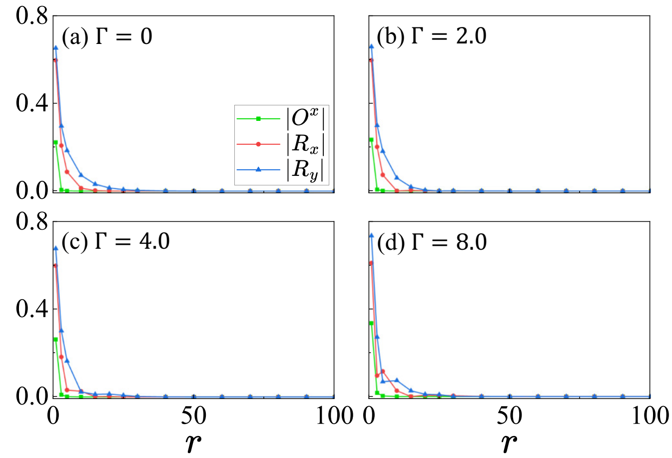

FIG. 11. The long-distance behaviors of string order parameter $|O^x|$ and spin correlation function $|R_x|$, $|R_y|$ for (a) $\Gamma = 0$, (b) $\Gamma = 2.0$, (c) $\Gamma = 4.0$, and (d) $\Gamma = 8.0$. Throughout, $\lambda_x = -3$, $\lambda_y = 3$.

APPENDIX D: DETAILS ABOUT CORRELATION FUNCTIONS IN PM PHASE

In this Appendix, we provide the properties of correlation functions in the PM phase. As shown in Fig. 11, the results reveal that the string order parameter $|O^x|$ and the spin correlation function $|R_x|,\ |R_y|$ decay exponentially with the distance r increasing in the PM phase.

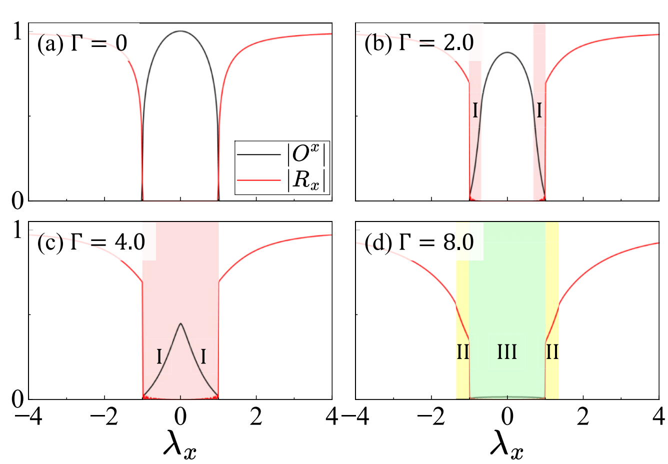

FIG. 12. The numerical results of string order parameter $|O^x|$, spin correlation function $|R_x|$ with respect to λ_x for (a) $\Gamma = 0$, (b) $\Gamma = 2.0$, (c) $\Gamma = 4.0$, and (d) $\Gamma = 8.0$. The red, yellow, green shadings correspond to critical region I, II, Luttinger liquid-like phase, respectively. Throughout, $\lambda_y = 0$, $r = 1000$.

APPENDIX E: DISTRIBUTION OF ORDER PARAMETERS VERSUS λ_x

In this section, we present additional data on the distribution of the order parameters of $|O^x|$, $|R_x|$ versus λ_x when $\lambda_y = 0$. In the Hermitian case ($\Gamma = 0$), when $\lambda_x > 1$ ($\lambda_x < 1$), $|R_x|$ is nonzero, indicating that the system resides in the $\mathrm{AFM_x}$ ($\mathrm{FM_x}$) phase in such a parameter region [see Fig. 12(a)]. When $-1 < \lambda_x < 1$, $|O^x|$ is nonzero, suggesting that the region is in the cluster SPT phase [see Fig. 12(a)].

Then, we investigate the non-Hermitian case. Under the condition of $\Gamma = 2$, as shown in Fig. 12(b), in critical region I, $|O^x|$ is nonzero. As the dissipation intensity increases, the range of each phase changes. When the dissipation intensity increases to $\Gamma = 4$ [see Fig. 12(c)], the SPT phase disappears completely, which is in agreement with the behavior in the phase diagram [see Fig. 2(c)]. Under the condition of $\Gamma = 8.0$, it can be seen that the spin correlation function $|R_x|$ is a limited value in the critical region II [see Fig. 12(d)].

[1] B. Yang, H. Sun, C.-J. Huang, H.-Y. Wang, Y. Deng, H.-N. Dai, Z.-S. Yuan, and J.-W. Pan, Cooling and entangling ultracold atoms in optical lattices, Science **369**, 550 (2020).

[2] Z. Meng, L. Wang, W. Han, F. Liu, K. Wen, C. Gao, P. Wang, C. Chin, and J. Zhang, Atomic bose–einstein condensate in twisted-bilayer optical lattices, Nature (London) **615**, 231 (2023).

[3] D. Jaksch, C. Bruder, J. I. Cirac, C. W. Gardiner, and P. Zoller, Cold bosonic atoms in optical lattices, Phys. Rev. Lett. **81**, 3108 (1998).

[4] D.-W. Zhang, Y. X. Zhao, R.-B. Liu, Z.-Y. Xue, S.-L. Zhu, and Z. D. Wang, Quantum simulation of exotic $\mathcal{PT}$-invariant topological nodal loop bands with ultracold atoms in an optical lattice, Phys. Rev. A **93**, 043617 (2016).

[5] S.-L. Zhu, Z.-D. Wang, Y.-H. Chan, and L.-M. Duan, Topological bose-mott insulators in a one-dimensional optical superlattice, Phys. Rev. Lett. **110**, 075303 (2013).

[6] S.-L. Zhu, B. Wang, and L.-M. Duan, Simulation and detection of Dirac fermions with cold atoms in an optical lattice, Phys. Rev. Lett. **98**, 260402 (2007).

[7] S.-L. Zhu, H. Fu, C.-J. Wu, S.-C. Zhang, and L.-M. Duan, Spin hall effects for cold atoms in a light-induced gauge potential, Phys. Rev. Lett. **97**, 240401 (2006).

[8] L. B. Shao, S.-L. Zhu, L. Sheng, D. Y. Xing, and Z. D. Wang, Realizing and detecting the quantum hall effect without landau levels by using ultracold atoms, Phys. Rev. Lett. **101**, 246810 (2008).

[9] S.-C. Ji, J.-Y. Zhang, L. Zhang, Z.-D. Du, W. Zheng, Y.-J. Deng, H. Zhai, S. Chen, and J.-W. Pan, Experimental determination of the finite-temperature phase diagram of a spin–orbit coupled bose gas, Nat. Phys. **10**, 314 (2014).

[10] H.-Y. Wang, W.-Y. Zhang, Z. Yao, Y. Liu, Z.-H. Zhu, Y.-G. Zheng, X.-K. Wang, H. Zhai, Z.-S. Yuan, and J.-W. Pan, Interrelated thermalization and quantum criticality in a lattice gauge simulator, Phys. Rev. Lett. **131**, 050401 (2023).

[11] M. Greiner, O. Mandel, T. Esslinger, T. W. Hänsch, and I. Bloch, Quantum phase transition from a superfluid to a mott insulator in a gas of ultracold atoms, Nature (London) **415**, 39 (2002).

[12] X. Zhang, Y. Chen, Z. Wu, J. Wang, J. Fan, S. Deng, and H. Wu, Observation of a superradiant quantum phase transition in an intracavity degenerate fermi gas, Science **373**, 1359 (2021).

[13] S. Sunami, V. P. Singh, D. Garrick, A. Beregi, A. J. Barker, K. Luksch, E. Bentine, L. Mathey, and C. J. Foot, Universal scaling of the dynamic bkt transition in quenched 2d bose gases, Science **382**, 443 (2023).

[14] T. Xiao, D. Xie, Z. Dong, T. Chen, W. Yi, and B. Yan, Observation of topological phase with critical localization in a quasi-periodic lattice, Sci. Bull. **66**, 2175 (2021).

[15] C. Gross and I. Bloch, Quantum simulations with ultracold atoms in optical lattices, Science **357**, 995 (2017).

[16] D. Xie, T.-S. Deng, T. Xiao, W. Gou, T. Chen, W. Yi, and B. Yan, Topological quantum walks in momentum space with a bose-einstein condensate, Phys. Rev. Lett. **124**, 050502 (2020).

[17] S. O. Skrøvseth and S. D. Bartlett, Phase transitions and localizable entanglement in cluster-state spin chains with ising couplings and local fields, Phys. Rev. A **80**, 022316 (2009).

[18] L. C. Venuti and M. Roncaglia, Analytic relations between localizable entanglement and string correlations in spin systems, Phys. Rev. Lett. **94**, 207207 (2005).

[19] M. Popp, F. Verstraete, M. A. Martín-Delgado, and J. I. Cirac, Localizable entanglement, Phys. Rev. A **71**, 042306 (2005).

[20] J. K. Pachos and M. B. Plenio, Three-spin interactions in optical lattices and criticality in cluster hamiltonians, Phys. Rev. Lett. **93**, 056402 (2004).

[21] C. Becker, P. Soltan-Panahi, J. Kronjäger, S. Dörscher, K. Bongs, and K. Sengstock, Ultracold quantum gases in triangular optical lattices, New J. Phys. **12**, 065025 (2010).

[22] P. Smacchia, L. Amico, P. Facchi, R. Fazio, G. Florio, S. Pascazio, and V. Vedral, Statistical mechanics of the cluster ising model, Phys. Rev. A **84**, 022304 (2011).

[23] C. Ding, Phase transitions of a cluster ising model, Phys. Rev. E **100**, 042131 (2019).

[24] W. Son, L. Amico, R. Fazio, A. Hamma, S. Pascazio, and V. Vedral, Quantum phase transition between cluster and antiferromagnetic states, Europhys. Lett. **95**, 50001 (2011).

[25] W. Nie, F. Mei, L. Amico, and L. C. Kwek, Scaling of geometric phase versus band structure in cluster-ising models, Phys. Rev. E **96**, 020106(R) (2017).

[26] S. M. Giampaolo and B. C. Hiesmayr, Topological and nematic ordered phases in many-body cluster-ising models, Phys. Rev. A **92**, 012306 (2015).

[27] Z.-X. Guo, X.-J. Yu, X.-D. Hu, and Z. Li, Emergent phase transitions in a cluster ising model with dissipation, Phys. Rev. A **105**, 053311 (2022).

[28] X.-J. Yu, S. Yang, H.-Q. Lin, and S.-K. Jian, Universal entanglement spectrum in one-dimensional gapless symmetry protected topological states, Phys. Rev. Lett. **133**, 026601 (2024).

[29] X.-J. Yu and W.-L. Li, Fidelity susceptibility at the lifshitz transition between the noninteracting topologically distinct quantum critical points, Phys. Rev. B **110**, 045119 (2024).

[30] H.-L. Zhang, H.-Z. Li, S. Yang, and X.-J. Yu, Quantum phase transition and critical behavior between the gapless topological phases, Phys. Rev. A **109**, 062226 (2024).
[31] S. Yang, H.-Q. Lin, and X.-J. Yu, Gapless topological behaviors in a long-range quantum spin chain, Commun. Phys. **8**, 27 (2025).
[32] X.-J. Yu, R.-Z. Huang, H.-H. Song, L. Xu, C. Ding, and L. Zhang, Conformal boundary conditions of symmetry-enriched quantum critical spin chains, Phys. Rev. Lett. **129**, 210601 (2022).
[33] R. K. Malakar and A. K. Ghosh, Quantum phases of spin-1/2 extended xy model in transverse magnetic field, Phys. Scr. **99**, 035944 (2024).
[34] R. K. Malakar and A. K. Ghosh, Magnetic phases of xy model with three-spin terms: interplay of topology and entanglement, J. Phys.: Condens. Matter **36**, 325401 (2024).
[35] W.-H. Zhong, W.-L. Li, Y.-C. Chen, and X.-J. Yu, Topological edge modes and phase transitions in a critical fermionic chain with long-range interactions, Phys. Rev. A **110**, 022212 (2024).
[36] J. Li, A. K. Harter, J. Liu, L. de Melo, Y. N. Joglekar, and L. Luo, Observation of parity-time symmetry breaking transitions in a dissipative floquet system of ultracold atoms, Nat. Commun. **10**, 855 (2019).
[37] H. Schwager, J. I. Cirac, and G. Giedke, Dissipative spin chains: Implementation with cold atoms and steady-state properties, Phys. Rev. A **87**, 022110 (2013).
[38] Q. Liang, D. Xie, Z. Dong, H. Li, H. Li, B. Gadway, W. Yi, and B. Yan, Dynamic signatures of non-Hermitian skin effect and topology in ultracold atoms, Phys. Rev. Lett. **129**, 070401 (2022).
[39] S. Goto and I. Danshita, Measurement-induced transitions of the entanglement scaling law in ultracold gases with controllable dissipation, Phys. Rev. A **102**, 033316 (2020).
[40] K. Yamamoto, M. Nakagawa, N. Tsuji, M. Ueda, and N. Kawakami, Collective excitations and nonequilibrium phase transition in dissipative fermionic superfluids, Phys. Rev. Lett. **127**, 055301 (2021).
[41] L.-L. Yan, J.-W. Zhang, M.-R. Yun, J.-C. Li, G.-Y. Ding, J.-F. Wei, J.-T. Bu, B. Wang, L. Chen, S.-L. Su, F. Zhou, Y. Jia, E.-J. Liang, and M. Feng, Experimental verification of dissipation-time uncertainty relation, Phys. Rev. Lett. **128**, 050603 (2022).
[42] D. C. Cole, S. D. Erickson, G. Zarantonello, K. P. Horn, P.-Y. Hou, J. J. Wu, D. H. Slichter, F. Reiter, C. P. Koch, and D. Leibfried, Resource-efficient dissipative entanglement of two trapped-ion qubits, Phys. Rev. Lett. **128**, 080502 (2022).
[43] J.-W. Zhang, J.-Q. Zhang, G.-Y. Ding, J.-C. Li, J.-T. Bu, B. Wang, L.-L. Yan, S.-L. Su, L. Chen, F. Nori, Ş. K. Özdemir, F. Zhou, H. Jing, and M. Feng, Dynamical control of quantum heat engines using exceptional points, Nat. Commun. **13**, 6225 (2022).
[44] S. Longhi, Incoherent non-Hermitian skin effect in photonic quantum walks, Light Sci. Appl. **13**, 95 (2024).
[45] X.-R. Ma, K. Cao, X.-R. Wang, Z. Wei, Q. Du, and S.-P. Kou, Non-Hermitian chiral skin effect, Phys. Rev. Res. **6**, 013213 (2024).
[46] H. Zhang, T. Chen, L. Li, C. H. Lee, and X. Zhang, Electrical circuit realization of topological switching for the non-Hermitian skin effect, Phys. Rev. B **107**, 085426 (2023).
[47] G. Xu, X. Zhou, Y. Li, Q. Cao, W. Chen, Y. Xiao, L. Yang, and C.-W. Qiu, Non-Hermitian chiral heat transport, Phys. Rev. Lett. **130**, 266303 (2023).
[48] X. Shu, Q. Zhong, K. Hong, O. You, J. Wang, G. Hu, A. Alù, S. Zhang, D. N. Christodoulides, and L. Chen, Chiral transmission by an open evolution trajectory in a non-Hermitian system, Light Sci. Appl. **13**, 65 (2024).
[49] C. Yin, H. Jiang, L. Li, R. Lü, and S. Chen, Geometrical meaning of winding number and its characterization of topological phases in one-dimensional chiral non-Hermitian systems, Phys. Rev. A **97**, 052115 (2018).
[50] W. Chen, Ş. Kaya Özdemir, G. Zhao, J. Wiersig, and L. Yang, Exceptional points enhance sensing in an optical microcavity, Nature (London) **548**, 192 (2017).
[51] A. Li, H. Wei, M. Cotrufo, W. Chen, S. Mann, X. Ni, B. Xu, J. Chen, J. Wang, S. Fan, C.-W. Qiu, A. Alù, and L. Chen, Exceptional points and non-Hermitian photonics at the nanoscale, Nat. Nanotechnol. **18**, 706 (2023).
[52] M.-A. Miri and A. Alù, Exceptional points in optics and photonics, Science **363**, eaar7709 (2019).
[53] B. Zhen, C. W. Hsu, Y. Igarashi, L. Lu, I. Kaminer, A. Pick, S.-L. Chua, J. D. Joannopoulos, and M. Soljačić, Spawning rings of exceptional points out of Dirac cones, Nature (London) **525**, 354 (2015).
[54] S.-Z. Li and Z. Li, Ring structure in the complex plane: A fingerprint of a non-Hermitian mobility edge, Phys. Rev. B **110**, L041102 (2024).
[55] G.-J. Liu, J.-M. Zhang, S.-Z. Li, and Z. Li, Emergent strength-dependent scale-free mobility edge in a nonreciprocal long-range Aubry-André-Harper model, Phys. Rev. A **110**, 012222 (2024).
[56] X.-J. Yu, Z. Pan, L. Xu, and Z.-X. Li, Non-Hermitian strongly interacting Dirac fermions, Phys. Rev. Lett. **132**, 116503 (2024).
[57] S.-Z. Li, X.-J. Yu, and Z. Li, Emergent entanglement phase transitions in non-Hermitian Aubry-André-Harper chains, Phys. Rev. B **109**, 024306 (2024).
[58] H.-Z. Li, X.-J. Yu, and J.-X. Zhong, Non-Hermitian stark many-body localization, Phys. Rev. A **108**, 043301 (2023).
[59] K.-Q. Huang, W.-L. Li, W.-L. Zhao, and Z. Li, Characterizing entanglement in non-Hermitian chaotic systems via out-of-time ordered correlators, Chin. Phys. B **31**, 090301 (2022).
[60] Y.-G. Liu, L. Xu, and Z. Li, Quantum phase transition in a non-Hermitian *XY* spin chain with global complex transverse field, J. Phys.: Condens. Matter **33**, 295401 (2021).
[61] K.-Q. Huang, W.-L. Zhao, and Z. Li, Effective protection of quantum coherence by a non-Hermitian driving potential, Phys. Rev. A **104**, 052405 (2021).
[62] X. Shen, F. Wang, Z. Li, and Z. Wu, Landau-Zener-Stückelberg interferometry in $\mathcal{PT}$-symmetric non-Hermitian models, Phys. Rev. A **100**, 062514 (2019).
[63] P. He, J.-H. Fu, D.-W. Zhang, and S.-L. Zhu, Double exceptional links in a three-dimensional dissipative cold atomic gas, Phys. Rev. A **102**, 023308 (2020).
[64] P. He, H.-T. Ding, and S.-L. Zhu, Geometry and superfluidity of the flat band in a non-Hermitian optical lattice, Phys. Rev. A **103**, 043329 (2021).

[65] P. He, Y.-G. Liu, J.-T. Wang, and S.-L. Zhu, Damping transition in an open generalized Aubry-André-Harper model, Phys. Rev. A **105**, 023311 (2022).
[66] J.-R. Li, L.-L. Zhang, W.-B. Cui, and W.-J. Gong, Topological properties in non-Hermitian tetratomic Su-Schrieffer-Heeger lattices, Phys. Rev. Res. **4**, 023009 (2022).
[67] H.-Q. Liang and L. Li, Topological properties of non-Hermitian creutz ladders, Chin. Phys. B **31**, 010310 (2022).
[68] Z. Gong, Y. Ashida, K. Kawabata, K. Takasan, S. Higashikawa, and M. Ueda, Topological phases of non-Hermitian systems, Phys. Rev. X **8**, 031079 (2018).
[69] T. Liu, Y.-R. Zhang, Q. Ai, Z. Gong, K. Kawabata, M. Ueda, and F. Nori, Second-order topological phases in non-Hermitian systems, Phys. Rev. Lett. **122**, 076801 (2019).
[70] M. Ezawa, Non-Hermitian higher-order topological states in nonreciprocal and reciprocal systems with their electric-circuit realization, Phys. Rev. B **99**, 201411(R) (2019).
[71] E. Edvardsson, F. K. Kunst, and E. J. Bergholtz, Non-Hermitian extensions of higher-order topological phases and their biorthogonal bulk-boundary correspondence, Phys. Rev. B **99**, 081302(R) (2019).
[72] X.-W. Luo and C. Zhang, Higher-order topological corner states induced by gain and loss, Phys. Rev. Lett. **123**, 073601 (2019).
[73] D.-W. Zhang, L.-Z. Tang, L.-J. Lang, H. Yan, and S.-L. Zhu, Non-Hermitian topological anderson insulators, Sci. China: Phys., Mech. Astron. **63**, 267062 (2020).
[74] M. Müller, S. Diehl, G. Pupillo, and P. Zoller, Engineered open systems and quantum simulations with atoms and ions, Adv. At. Mol. Opt. Phys. **61**, 1 (2012).
[75] J. M. Zeuner, M. C. Rechtsman, Y. Plotnik, Y. Lumer, S. Nolte, M. S. Rudner, M. Segev, and A. Szameit, Observation of a topological transition in the bulk of a non-Hermitian system, Phys. Rev. Lett. **115**, 040402 (2015).
[76] T. E. Lee and C.-K. Chan, Heralded magnetism in non-Hermitian atomic systems, Phys. Rev. X **4**, 041001 (2014).
[77] G. C. Wick, The evaluation of the collision matrix, Phys. Rev. **80**, 268 (1950).
[78] E. Barouch and B. M. McCoy, Statistical mechanics of the XY model. II. Spin-correlation functions, Phys. Rev. A **3**, 786 (1971).
[79] F. Pollmann and A. M. Turner, Detection of symmetry-protected topological phases in one dimension, Phys. Rev. B **86**, 125441 (2012).
[80] J. Haegeman, D. Pérez-García, I. Cirac, and N. Schuch, Order parameter for symmetry-protected phases in one dimension, Phys. Rev. Lett. **109**, 050402 (2012).
[81] A. M. Turner, F. Pollmann, and E. Berg, Topological phases of one-dimensional fermions: An entanglement point of view, Phys. Rev. B **83**, 075102 (2011).
[82] R. Verresen, R. Thorngren, N. G. Jones, and F. Pollmann, Gapless topological phases and symmetry-enriched quantum criticality, Phys. Rev. X **11**, 041059 (2021).
[83] S. Montes and A. Hamma, Phase diagram and quench dynamics of the cluster-xy spin chain, Phys. Rev. E **86**, 021101 (2012).
[84] M. B. Plenio and P. L. Knight, The quantum-jump approach to dissipative dynamics in quantum optics, Rev. Mod. Phys. **70**, 101 (1998).
[85] H. Carmichael, *An Open Systems Approach to Quantum Optics* (Springer, New York, 1993).
[86] R. Dum, P. Zoller, and H. Ritsch, Monte carlo simulation of the atomic master equation for spontaneous emission, Phys. Rev. A **45**, 4879 (1992).
[87] J. Dalibard, Y. Castin, and K. Mølmer, Wave-function approach to dissipative processes in quantum optics, Phys. Rev. Lett. **68**, 580 (1992).
[88] A. J. Daley, Quantum trajectories and open many-body quantum systems, Adv. Phys. **63**, 77 (2014).
[89] H.-P. Breuer and F. Petruccione, *The Theory of Open Quantum Systems* (Oxford University Press, New York, 2007).
[90] Á. Rivas and S. F. Huelga, *Open Quantum Systems: An Introduction* (Springer, New York, 2011).
[91] A. Dutta, G. Aeppli, B. K. Chakrabarti, U. Divakaran, T. F. Rosenbaum, and D. Sen, *Quantum Phase Transitions in Transverse Field Spin Models: From Statistical Physics to Quantum Information* (Cambridge University Press, Cambridge, England, 2015).